



SAPIENZA  
UNIVERSITÀ DI ROMA

## Mesoscale Atmospheric Circulation and Severe Weather

Facoltà di Scienze Matematiche Fisiche e Naturali  
Dipartimento di Fisica  
Corso di Laurea in Fisica

**Matteo Cheri**

ID number 1686219

Advisor

Anna Maria Siani

External Advisor

Serena Falasca

Academic Year 2024/2025

Thesis defended on 26 June 2025  
in front of a Board of Examiners composed by:

Carlo Mariani (chairman)

Stefano Lupi

Marco Nardecchia

Dominik Schleicher

Matteo Negri

Alessandra Betti

Edoardo Milanetti

---

**Mesoscale Atmospheric Circulation and Severe Weather**  
BSc Thesis. Sapienza University of Rome

© 2025 Matteo Cheri. All rights reserved

This thesis has been typeset by L<sup>A</sup>T<sub>E</sub>X and the Sapthesis class.

Author's email: cheri.1686219@studenti.uniroma1.it

# Contents

---

<b>1</b>	<b>Introduction</b>	<b>5</b>
<b>2</b>	<b>Fundamental Equations</b>	<b>6</b>
2.1	Atmospheric Scales . . . . .	6
2.2	Governing Equations of Mesoscale Dynamics . . . . .	7
2.2.1	Approximations to the Governing Equations . . . . .	8
2.2.2	Vorticity and Potential Vorticity . . . . .	9
<b>3</b>	<b>Orographic Flows</b>	<b>10</b>
3.1	Mountain Waves . . . . .	10
3.1.1	Linear Theory . . . . .	10
3.1.2	Mountain Waves with Variable Scorer Parameter . . . . .	12
3.2	Flow over Mesoscale Mountain Ranges . . . . .	13
3.2.1	Alpine Lee Cyclogenesis . . . . .	13
<b>4</b>	<b>Severe Storms</b>	<b>15</b>
4.1	Cumulus Convection . . . . .	15
4.1.1	Buoyancy Pressure Perturbation . . . . .	15
4.1.2	Dynamic Pressure and Vorticity Perturbations . . . . .	16
4.1.3	Cumulonimbus Clouds and Storm Categorization . . . . .	16
4.2	Supercell Storms . . . . .	18
4.2.1	Storm Strength . . . . .	18
4.2.2	Storm Splitting . . . . .	19
4.2.3	Updraft Rotation and Supercell Tornadogenesis . . . . .	19
<b>5</b>	<b>Front and Jet Dynamics</b>	<b>22</b>
5.1	Frontogenesis . . . . .	22
5.1.1	Thermodynamics and Kinematics of Frontogenesis . . . . .	22
5.1.2	Cross-frontal Circulations and the Sawyer-Eliassen Equation	22
5.2	Jet Streaks . . . . .	24
5.2.1	Jetogenesis and Lateral Secondary Circulations . . . . .	24
5.2.2	Upper-Lower Level Jet Streak Coupling and Severe Storms .	25
<b>6</b>	<b>Conclusions</b>	<b>27</b>

---

<b>A Additional Figures</b>	<b>29</b>
A.1 Orographic Flows . . . . .	29
A.2 Severe Storms . . . . .	30

# 1. Introduction

---

The study of mesoscale circulations in the atmosphere is a fundamental tool for forecasting and analyzing atmospheric phenomena and severe weather events in the sub-synoptic scale, where orography and localized (even strong) perturbations become non-negligible in the evaluation of the fundamental equations of fluid dynamics.

The following thesis studies the governing equations of fluid dynamics in the atmospheric medium and finds the necessary approximations for evaluating events in the mesoscale via separating the equations into a base state in thermodynamic and geostrophic equilibrium and a perturbative state, which describes the perturbations encountered in this scale.

Further approximations are found by imposing consideration on the parameters and rewriting the continuity equation, as the deep convection and shallow convection continuity equation. A brief description of vorticity and the conservation of Ertel potential vorticity are then expressed.

The second chapter treats mesoscale flows over orography, considering the solution of the Scorer equation in the linear regime and with variable Scorer parameters [1]. Flow over mesoscale mountain ranges is then studied with particular concentration on Alpine cyclogenesis, researched in the ALPEX expedition by Tibaldi et. al [2].

The third chapter describes cumulus convection, the dynamics of the formation of cumulonimbus clouds and storm categorization, concentrating on the dynamics of supercell storms, which are known to be the main drive of severe thunderstorms, flash flooding, large hailstorms and tornadoes. A mathematical framework of storm splitting in high-shear environments is given and the phenomenology of supercell tornadogenesis is then described.

The last chapter treats the mesoscale dynamics of frontogenesis by using the wedge model of fronts and the Miller frontogenesis [3]. Cross-frontal circulations are then treated by using the quasi-geostrophic approximation and the Sawyer-Eliassen equation [4, 5] is derived on the vertical plane of the front, and the elliptic condition for the potential vorticity is given. Jet streams are then derived as a high-level analog of fronts and lateral secondary circulations are described, with the last section reserved for describing upper and lower jet coupling and its part in severe weather outbreaks in the plains of central north America and Argentina [6]

## 2. Fundamental Equations

---

### § 2.1 Atmospheric Scales

---

Due to the complexity of the atmospheric system, different approximations must be used in order to explain and forecast atmospheric phenomena. Four main scales have been defined, as for [7, 8]

	Scale	Main Phenomena
Microscale	<2 km	Dust devils, eddies, turbulence
Mesoscale	2-2000 km	Storms, squall lines, fronts, tornadoes, breezes
Synoptic	>2000 km	Pressure systems, cyclones
Planetary	Global	Trade winds, el niño

**Table 2.1.** Atmospheric scales and the main phenomena at those levels

The mesoscale, which is the theme of this work, is further divided into three subscales

- Meso- $\alpha$ : 200-2000 km scale; scale of fronts, squall lines, mesoscale convective systems and tropical cyclones
- Meso- $\beta$ : 20-200 km scale of mesocyclones and breezes
- Meso- $\gamma$ : 2-20 km scale of thunderstorm convection and orographic flow

The atmospheric scales can also be defined in terms of the Lagrangian Rossby number  $R_o$  as in figure 2.1, adapted from Emanuel K. A., 1986 [9]

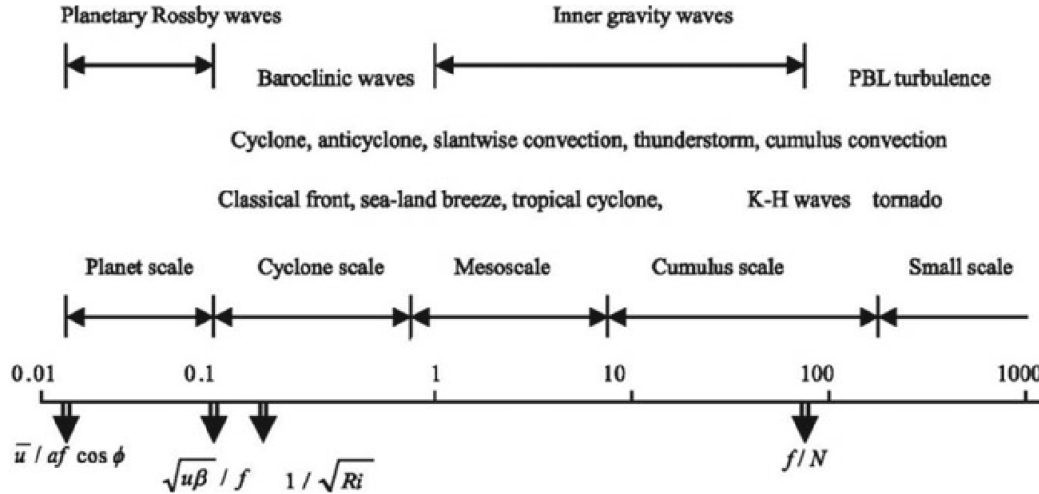


**Figure 2.1.** Definition of atmospheric scales in terms of the Lagrangian Rossby number  $R_o = 2\pi/fT$ , with  $T$  being the Lagrangian time scale (phenomena dependent), after [9]

## § 2.2 Governing Equations of Mesoscale Dynamics

The equations needed to describe mesoscale dynamics are those of a stratified inviscid fluid over a plane. These are the Navier-Stokes equations and the first law of thermodynamics, described as follows [7, 8]

$$\begin{aligned}
 \frac{\partial \mathbf{v}}{\partial t} + \mathbf{v} \cdot \nabla \mathbf{v} + f \hat{\mathbf{k}} \times \mathbf{v}_H &= -\frac{1}{\rho} \nabla p - \hat{\mathbf{k}} g + \mathbf{F}_r \\
 \frac{\partial \rho}{\partial t} + \mathbf{v} \cdot \nabla \rho + \rho \nabla \cdot \mathbf{v} &= 0 \\
 \frac{\partial \theta}{\partial t} + \mathbf{v} \cdot \nabla \theta &= \frac{\theta}{c_p T} \dot{q} = \dot{Q} \\
 p &= \rho R_d T \\
 \theta &= T \left( \frac{p_s}{p} \right)^{\frac{R_d}{c_p}}
 \end{aligned} \tag{2.1}$$

Where  $\mathbf{v} = (u, v, w)$  is the wind velocity field,  $\mathbf{v}_H = (u, v)$  is the horizontal wind velocity field,  $f$  is the Coriolis parameter,  $p$  the pressure field,  $\mathbf{F}_r$  are frictional forces,  $\rho$  is the density field,  $\theta$  the potential temperature,  $c$ ,  $R_d$  are the thermodynamic parameters for dry air and  $\dot{q}$  is the diabatic heating. The moist version of these equations is obtained by substituting the thermodynamic parameters and utilizing the virtual temperature.

In order to describe the atmospheric mesoscale, these equations can be linearized via partition into a base state  $\mathcal{A}_s$  and a mesoscale perturbation  $\mathcal{A}'$  as  $\mathcal{A}_s + \mathcal{A}'$ . The base state is assumed geostrophic and hydrostatic equilibrium, thus, the equa-

tions of the base state are

$$\begin{aligned} p_s &= \rho_s R_d T_s \\ \theta_s &= T_s \left( \frac{p_{surf}}{p_s} \right)^{\frac{R_d}{c_p}} \\ \mathbf{V} &= -\frac{1}{f\rho_s} \hat{\mathbf{k}} \times \nabla_H p_s \\ \frac{\partial \rho_s}{\partial t} + \mathbf{V} \cdot \nabla \rho_s + \rho_s \nabla \cdot \mathbf{V} &= \frac{1}{c_s^2} \mathbf{V} \cdot \nabla_H p_s = 0 \\ \mathbf{V} \cdot \nabla_H \theta_s &= 0 \end{aligned} \quad (2.2)$$

Where  $\mathbf{V} = (U, V)$  is the geostrophic base wind and  $\nabla_H = (\partial_x, \partial_y)$  are the horizontal components of the gradient operator.

Under these conditions it's immediate to see that the base state equations imply thermal wind balance

$$\mathbf{v}_T = \frac{\partial \mathbf{V}}{\partial z} = -\frac{g}{f\theta_s} \hat{\mathbf{k}} \times \nabla_H \theta_s$$

Applying the perturbative equations to (2.1), imposing the equations of the base state (2.2) and ignoring nonlinear terms we obtain the equations fo the mesoscale perturbations

$$\begin{aligned} \frac{\partial \mathbf{v}'}{\partial t} + \mathbf{V} \cdot \nabla_H \mathbf{v}' + w' \frac{\partial \mathbf{V}}{\partial z} + f\hat{\mathbf{k}} \times \mathbf{v}'_H + \frac{1}{\rho_s} \nabla p' - g \frac{\theta'}{\theta_s} \hat{\mathbf{k}} + \frac{p'}{\rho_s H} \hat{\mathbf{k}} &= 0 \\ \frac{1}{c_s^2} \left( \frac{\partial p'}{\partial t} + \mathbf{V} \cdot \nabla_H p' + \rho_s f (Vu' - Uv') \right) - \frac{\rho_s}{H} w' + p_s \nabla \cdot \mathbf{v}' &= \frac{\rho_s}{c_p T_s} q' \quad (2.3) \\ \frac{\partial \theta'}{\partial t} + \mathbf{V} \cdot \nabla_H \theta' + \frac{f\theta_s}{g} \left( \frac{\partial V}{\partial z} u' - \frac{\partial U}{\partial z} v' \right) + \frac{N^2 \theta_s}{g} w' &= \frac{\theta_s}{c_p T_s} q' \end{aligned}$$

Where  $c_s = \sqrt{\gamma R_d T}$  is the speed of sound,  $N = \sqrt{g \partial_z \log \theta_s}$  is the Brunt-Väisälä frequency and  $H = c_s^2/g$  is the scale height.

### §§ 2.2.1 Approximations to the Governing Equations

The equations (2.3) form an elastic fluid system which can include different type of waves depending on the approximations made on  $f, c_s$  (acoustic, acoustic-gravity, gravity and inertia-gravity), while the general system (2.1) may include static, shear, symmetric, inertial and baroclinic instabilities. These equations can be initially approximated by assuming that  $c_s, H$  are height-independent. The continuity equation obtained, known as the deep convection continuity equation reads as follows

$$\nabla \cdot (\mathbf{v}' e^{-\frac{z}{H}}) = 0 \quad (2.4)$$

If the vertical scale of the disturbance is significantly smaller than the scale height, we can approximate the deep convection continuity equation to the incompressible or shallow convection continuity equation  $\nabla \cdot \mathbf{v}' = 0$ .

The hydrodynamic equations can be approximated with the pseudo-incompressible

approximation, thus, defined the Exner function  $\pi = T/\theta$  and the heating rate per unit volume  $\dot{Q}$ , for an inviscid rotating flow we obtain, from equations (2.3)

$$\begin{aligned} \frac{\partial \mathbf{v}}{\partial t} + \mathbf{v} \cdot \nabla \mathbf{v} + \hat{\mathbf{k}} \times \mathbf{v}_H + c_p \theta \nabla \pi' &= 0 \\ \nabla \cdot (\rho_s \theta_s \mathbf{v}) &= \frac{\dot{Q}}{c_p \pi_s} \\ \frac{\partial \theta}{\partial t} + \mathbf{v} \cdot \nabla \theta &= \frac{\theta \dot{Q}}{c_p \pi_s \rho_s \theta_s} \end{aligned} \quad (2.5)$$

The equations can be approximated further considering the atmosphere as a Boussinesq fluid, which is equivalent to considering a hydrostatic approximation, where  $\rho_0, \theta_0$  are the Boussinesq parameters of the fluid

$$\frac{\partial p'}{\partial z} = \left( \frac{g \rho_0}{\theta_0} \right) \theta' \quad (2.6)$$

### §§ 2.2.2 Vorticity and Potential Vorticity

Defined the *vorticity* as  $\boldsymbol{\omega} = \nabla \times \mathbf{v}$ , and indicating  $\zeta = \hat{\mathbf{k}} \cdot \boldsymbol{\omega}$ , it's possible to derive a new fundamental equation by taking the curl of the horizontal components of the Navier-Stokes equation, where  $\{f, g\}_H = \partial_x f \partial_y g - \partial_y f \partial_x g$  is the Poisson bracket[10]

$$\frac{\partial \zeta}{\partial t} + \mathbf{v} \cdot \nabla \zeta + (\zeta + f) \nabla_H \cdot \mathbf{v} + \left( \frac{\partial w}{\partial x} \frac{\partial v}{\partial z} - \frac{\partial w}{\partial y} \frac{\partial u}{\partial z} \right) + v \frac{\partial f}{\partial y} = \frac{1}{\rho^2} \{\rho, p\}_H \quad (2.7)$$

The equation, known as the *vorticity equation*, permits the definition of a fundamental conservation law. Considering an isoentropic thermodynamic coordinate system  $(\rho, p, \theta)$  for a potential adiabatic flow, it's demonstrable that

$$\frac{d}{dt} \left[ \frac{\boldsymbol{\omega} \cdot \nabla \theta}{\rho} \right] = \frac{dPV}{dt} = 0 \quad (2.8)$$

The quantity  $PV$  is known as the *Ertel potential vorticity*

# 3. Orographic Flows

---

Many mesoscale weather phenomena are directly tied to forced circulations over orography.

One event in particular is the formation of mountain waves<sup>1</sup>, where flow over mountains creates oscillations which can cause severe turbulence, making its prediction fundamental for aviation safety.

## § 3.1 Mountain Waves

---

### §§ 3.1.1 Linear Theory

The main theory of mountain waves can be explained by considering a 2D, steady-state, adiabatic, inviscid, non rotating Boussinesq flow over small amplitude sinusoidal mountains.

Considering the flow only in the  $xz$ -plane, the governing equations (2.3) become [8]

$$\left\{ \begin{array}{l} U \frac{\partial u'}{\partial x} + w' \frac{\partial U}{\partial z} + \frac{1}{\rho_0} \frac{\partial p'}{\partial x} = 0 \\ U \frac{\partial w'}{\partial x} - g \frac{\theta'}{\theta_0} + \frac{1}{\rho_0} \frac{\partial p'}{\partial z} = 0 \\ \frac{\partial u'}{\partial x} + \frac{\partial w'}{\partial z} = 0 \\ U \frac{\partial \theta'}{\partial x} + \frac{N^2 \theta_0}{g} w' = 0 \end{array} \right. \quad (3.1)$$

The previous equations were further reduced by R. S. Scorer [1, 11, 12] into the *Scorer equation*

$$\nabla^2 w' + l^2(z) w' = 0 \quad (3.2)$$

Where  $l(z)$  is known as the *Scorer parameter*, defined in [11] as

$$l^2(z) = \frac{N^2}{U^2} - \frac{1}{U} \frac{\partial^2 U}{\partial z^2} \quad (3.3)$$

Supposing that the base-state wind  $U$  and the Brunt-Väisälä frequency  $N$  do not change with height  $z$ , and the terrain is defined as a sinusoidal wave  $h(x)$

$$h(x) = h_m \sin(kx) \quad (3.4)$$

---

<sup>1</sup>Also known as lee waves due to their lee-side propagation

Where  $h_m$  is mountain height and  $k$  is mountain wavenumber. It's possible to write a Cauchy problem for the Scorer equation by noting that the slope of the streamlines must equal the slope of the mountains at  $z = 0$

$$\frac{w'}{U + u'} = \frac{dh}{dx} \implies w' \simeq U \frac{dh}{dx} \quad (3.5)$$

Where we considered a small amplitude mountain and  $U \gg u'$ .

The Cauchy problem in this case is

$$\begin{cases} \nabla^2 w' + l^2 w' = 0 \\ w'(x, 0) = Uh_m k \cos(kx) \end{cases} \quad (3.6)$$

Supposing by similarity a sinusoidal solution on the horizontal direction, one obtains a one dimensional second order ordinary differential equation on height  $z$

$$\frac{d^2 w_i}{dz^2} + (l^2 - k^2) w_i(z) = 0 \quad (3.7)$$

This equation has two possible cases, depending on  $k, l$ . In the first case of  $l^2 < k^2$ , after imposing upper boundedness, the solution is a vertically evanescent wave.

$$w'(x, z) = Uh_m k \cos(kx) e^{-z\sqrt{k^2 - l^2}} \quad (3.8)$$

In the second case of  $l^2 > k^2$ , indicating  $l^2 - k^2 = m^2$  the flow response is a vertical propagating oscillation with tilting

$$w'(x, z) = Uh_m k \cos(kx + mz) \quad (3.9)$$

Using the governing equation it's possible to obtain back the other variables and their behavior.

Thus, the flow response is totally determined via the Scorer parameter  $l$  and the mountain wavenumber  $k$ , explicitly giving 4 mountain wave regimes

1.  $l^2 \ll k^2$  potential flow region
2.  $l^2 < k^2$  evanescent mountain wave region
3.  $l^2 > k^2$  vertically propagating mountain wave region
4.  $l^2 \gg k^2$  hydrostatic wave region

Mountain waves can contribute to cloud formation due to forced lifting of air parcels, as shown in this mountain wave event over the Appenine mountain range the 14th of January of 2024 caused by strong southeasterly winds from central Europe, as forecasted by the Italian Air Force in the low level significative weather forecast in figure A.1



**Figure 3.1.** Rotor clouds over the interested region, Images from the Sentinel 2 satellite, L2A band, ground images taken from Google Earth (Landsat, Copernicus) [13]

### §§ 3.1.2 Mountain Waves with Variable Scorer Parameter

The complete evaluation of mountain wave comes only if we consider atmospheric stratification and vertical variations of the base state wind velocity  $U$ , giving in the most general case a height-dependent scorer parameter  $l(z)$ .

The mathematical idea for evaluating a solution to the complete Scorer equation lies in the use of Fourier transforms

Considering a one-sided Fourier transform from the  $x$  to the  $k$ -space, the Scorer equation remains similar to the previous situation of a simple sinusoidal mountain range.

$$\frac{\partial^2 \hat{w}}{\partial z^2} + (l^2(z) - k^2) \hat{w}(k, z) = 0 \quad (3.10)$$

Considering again a constant scorer parameter, the vertical solutions will give the same result as previously, while the horizontal solution will be the inverse one-sided Fourier transform.

Using the properties of the Fourier transform and using phasor notation for the

vertical waves

$$\begin{aligned} w'(x, z) &= \hat{\mathcal{F}}_k^{-1}[\hat{w}(k, z)](x) = \\ &= 2\Re \left\{ \int_0^l ikU\hat{h}(k)e^{iz\sqrt{k^2-l^2}+ikx}dk + \int_l^\infty ikU\hat{h}(k)e^{-iz\sqrt{k^2-l^2}+ikx}dk \right\} \end{aligned} \quad (3.11)$$

It's clear that the first integral indicates the vertically propagating wave, while the second integral is the evanescent wave solution of the Scorer equation.

For the general case of  $l \equiv l(z)$ , the solution can be approximated using the WKB approximation [8], and supposing

$$\hat{w}(k, z) = A(k, z)e^{i\varphi(k, z)} \quad (3.12)$$

Plugging everything into (3.10) and deriving, the WKB-approximated partial differential equation is

$$(l^2(z) - k^2)A(k, z) - A(k, z)\left(\frac{\partial\varphi}{\partial z}\right)^2 + i\left(A(k, z)\frac{\partial^2\varphi}{\partial z^2} + 2\frac{\partial A}{\partial z}\frac{\partial\varphi}{\partial z}\right) + \frac{\partial^2 A}{\partial z^2} = 0$$

Using the slow variability of the amplitude  $A$ , therefore  $\partial_z^2 A(k, z) \simeq 0$ , and the equation separates into

$$\begin{cases} \frac{\partial\varphi}{\partial z} = \sqrt{l^2(z) - k^2} \\ \frac{\partial}{\partial z}\left(A^2\frac{\partial\varphi}{\partial z}\right) = 0 \end{cases} \Rightarrow A^2\sqrt{l^2(z) - k^2} = \text{const.} \quad (3.13)$$

## § 3.2 Flow over Mesoscale Mountain Ranges

---

Forced orographic flows do not only pose safety hazard to aviation. Another phenomena, common in zone with mesoscale mountain ranges, is *lee cyclogenesis*. This phenomenon has been studied thoroughly in the Alpine region of Italy, where orographic flows over the alps cause the formation of cyclones over the Padanian plain in northern Italy. In this scenario, due to the big dimension of mountains, rotational effects cannot be neglected anymore, thus defining the rotational nature of the flow.

### §§ 3.2.1 Alpine Lee Cyclogenesis

The phenomenon briefly cited above has been studied both theoretically and on the field via the ALPEX expedition in 1982. Tibaldi et al. [2] summarized the general characteristics of this phenomena as follows:

1. The Alpine cyclogenesis often occurs in association with a synoptic scale through or cyclone interacting with the surrounding orography
2. The cyclone development happens before the strong thermals associated with cold frontal penetration

3. The scales of the cyclone are comparable to the Rossby deformation radius of the flow, and the interaction behaves as a high-low dipole
4. The cyclone formation is divided in two phases; one of rapid development where the cyclone is shallow, and a second later phase of slower development, but with the deepening of the cyclone to the whole troposphere with scale factor of the order of the Rossby deformation number.

The generating winds are known as *Vorderseiten* and *Überströmungs* depending on their direction<sup>2</sup>. Both are accompanied with blocking and flow splitting, causing *Bora* events in the Adriatic sea and *Mistral wind* events on the Rhone valley in the Lyon direction.

*Vorderseiten* winds flow directly south from the French plains, passing through the Pyrenees and turning towards the Alps, forming a wave over northern Corsica and the gulf of Genoa with a warm front generation on the Padanian plain, while *Überströmungs* wind flow from stratified higher levels directly over the Alps, forming the lee cyclone with occlusion and a cold front over the gulf of Genoa.

The main theoretical explanation comes from a quasi-geostrophic baroclinic wave which causes the cyclone. Considering thus a quasi-geostrophic rotating Boussinesq flow, from the potential vorticity equation we have the two following equations for thermal balance and flow motion [8]

$$\begin{cases} \left( \frac{\partial}{\partial t} + \mathbf{v}_g \cdot \nabla \right) \left[ \nabla^2 p + \frac{f^2}{N^2} \frac{\partial^2 p}{\partial z^2} \right] = 0 \\ \frac{\partial \theta}{\partial t} + \mathbf{v}_g \cdot \nabla \theta + w \frac{\partial \theta}{\partial z} = 0 \quad (z = 0) \end{cases} \quad (3.14)$$

Where  $\mathbf{v}_g = (u_g, v_g)$  is the geostrophic wind. Suppose now a perturbation to this state, where  $\mathbf{v}_g = \mathbf{v}(z) + \mathbf{v}'_g$ ,  $\mathbf{v}(z) = \mathbf{V} + z\partial_z \mathbf{v}$  and considered the Alpine range as a function  $h_m(x, y)$ , the perturbed equations become then

$$\begin{cases} \nabla^2 p' + \frac{f^2}{N^2} \frac{\partial^2 p'}{\partial z^2} = 0 \\ \left( \frac{\partial}{\partial t} + \mathbf{v}_g \cdot \nabla \right) \frac{\partial p'}{\partial z} - \mathbf{v} \cdot \nabla_H p' + \rho_0 N w' = 0 \\ w(0) = \mathbf{v} \cdot \nabla_H h_m \end{cases} \quad (3.15)$$

Solving numerically the equation it's possible, using linear theory of mountain waves, determine the transient and vertically propagating wave solutions, which are in agreement with observations on Alpine cyclogenesis, in which the growing baroclinic wave is able to extract energy from the shear flow. The subsequent instability is able to then generate a cyclone in the region.

---

<sup>2</sup>Vorderseiten-type winds flow southwesterly, Überströmungs-type winds flow northwesterly

# 4. Severe Storms

---

## § 4.1 Cumulus Convection

---

The formation of cumulus or convective clouds (Free Weather Cumulus, Towering Cumulus, Cumulonimbus) happens in localized regions where high buoyancy favors the vertical acceleration of air particles.

The development of convection favors buoyancy pressure perturbations, environmental air entrainment in the updraft, its rotation and dynamic pressure perturbations.

### §§ 4.1.1 Buoyancy Pressure Perturbation

Due to the small scales associated with cumulus convection, we can ignore Coriolis effects and friction, giving for a Boussinesq non-rotating flow [14]

$$\frac{\partial \mathbf{v}}{\partial t} + \mathbf{v} \cdot \nabla \mathbf{v} = -\frac{1}{\rho_s} \nabla p' + b \hat{\mathbf{k}}$$

Using  $\partial_t \rho_s = 0$ , applying the anelastic approximation of the continuity equation<sup>1</sup>  $\nabla \cdot (\rho_s \mathbf{v}) = 0$  and multiplying by  $\rho_s$  and taking the divergence of the previous equation, we get

$$\nabla^2 p' = \frac{\partial}{\partial z} (\rho_s b) - \nabla \cdot (\rho_s \mathbf{v} \cdot \nabla \mathbf{v}) \quad (4.1)$$

Where  $b$  is the buoyancy, defined as  $b = g(\theta'/\theta_s + 0.61q'_v - q_H)$ , with  $q'_v$  as the water vapor mixing ratio perturbation and  $q_H$  is the hydrometeor mixing ratio.

Considering a partial buoyancy perturbation perturbation and a dynamic pressure perturbation such that  $p' = p'_b + p'_d$ , we can split the previous equation into two second order PDEs

$$\begin{cases} \nabla^2 p'_b = \frac{\partial}{\partial z} (\rho_s b) \\ \nabla^2 p'_d = \nabla \cdot (\rho_s \mathbf{v} \cdot \nabla \mathbf{v}) \end{cases} \quad (4.2)$$

Noting the similarity of the first equation to electrostatics, it's possible to define a BPGA (Buoyancy Pressure Gradient Acceleration) field as  $\rho_s^{-1} \nabla p'_b$ , for which, at the maximum pressure buoyancy perturbation we will have  $b = -BPGA$ .

---

<sup>1</sup>Also known in literature as the deep convection continuity equation

### §§ 4.1.2 Dynamic Pressure and Vorticity Perturbations

Inside convective clouds, the presence of a locally intense vertical vorticity field  $\zeta'$  can be explained directly with the tilting of  $\omega_H$  crosswise from the updraft. Considering a constant base state wind  $U$  from the  $x$  direction (westerly), from the vorticity equation we have [14]

$$\frac{\partial \zeta'}{\partial t} + U \frac{\partial \zeta'}{\partial x} = \frac{\partial U}{\partial z} \frac{\partial w}{\partial y} \quad (4.3)$$

Thus favoring the formation of vortexes alongside the updraft, in particular we will have  $\zeta' > 0$  south and  $\zeta' < 0$  north of the updraft.

From observations it's clear that the presence of windshear will favor the vorticity perturbation. This can be explained via nonlinear effects added to the vorticity equations in terms of stretching, as

$$\frac{\partial \zeta'}{\partial t} + U \frac{\partial \zeta'}{\partial x} \approx \frac{\partial U}{\partial z} \frac{\partial w}{\partial y} + \zeta' \frac{\partial w}{\partial z} \quad (4.4)$$

This also favors the production of dynamic pressure perturbations via shearing on the flanks of the updraft.

### §§ 4.1.3 Cumulonimbus Clouds and Storm Categorization

The most notable convective cloud is the cumulonimbus, a cloud associated with severe weather phenomena. It is formed via cumulus convection in strong updraft environments, which bring humid air parcels above the freezing layer favoring rain and hail in some cases, as depicted in figure 4.1, with an indication of the three stages of the cloud. Its shape is easily recognizable due to the presence of cloud turrets in the developing side and a high altitude anvil, formed by ice pellets dispersed horizontally by the breakdown of the updraft.

An example of a mature cumulonimbus cloud is depicted in the photographs 4.2

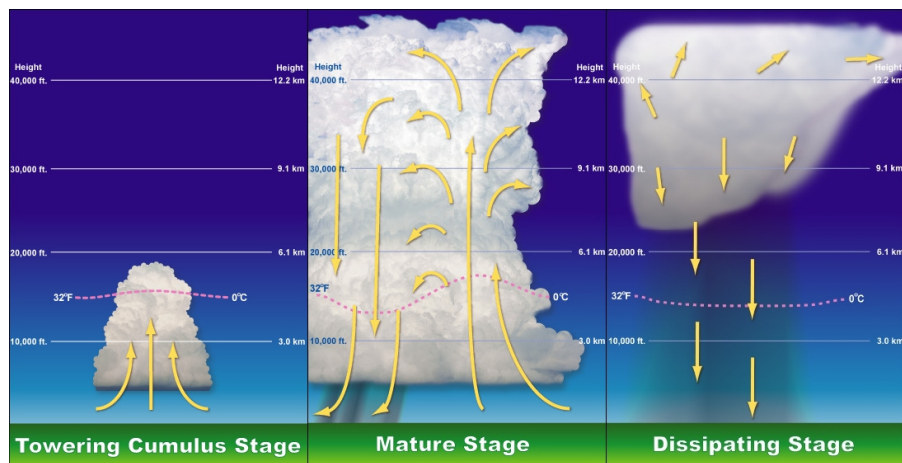


Figure 4.1. Stages of formation of a Cumulonimbus cloud [15]

The storms that can form are of three typologies, as for [8]:

1. Isolated or single cell storms, small in size and with only one updraft

2. Multicell storms, large and with multiple updrafts
3. Supercell storms, large but with a single very strong updraft, associated with extreme weather such as downbursts, large hail and tornadoes



**Figure 4.2.** Two photos of a mature cumulonimbus cloud over the northern Czech Republic, 15 June 2016. The anvil, also known as incus, of the cumulonimbus is evident, and shows a secondary precipitation of ice pellets known as virga. Photo by Michal Janoušek, Amatérská Meteorologická Společnost [16, 17]

## § 4.2 Supercell Storms

---

### §§ 4.2.1 Storm Strength

Supercell storms are one of the most violent storms that form. The study of the dynamics of supercells is fundamental for forecasting extreme weather phenomena, such as downbursts, large hail, severe thunderstorms, severe rain and tornadoes.

The single very strong updraft is notable in RADAR reflectivity maps, forming a WER (Weak Echo Region) or BWER (Bounded Weak Echo Region), also known as vault, thanks to its capacity of lifting to very high levels air parcels, not favoring drop formation and thus causing low reflectivity in the interested zone.

Their formation is favored by the presence of convective energy in the troposphere. Letting  $w_c$  as the vertical wind speed inside the storm, we have [14]

$$\frac{d}{dz} \left( \frac{1}{2} w_c^2 \right) = g \frac{T_c - T_{env}}{T_{env}} \quad (4.5)$$

We can define CAPE (Convective Available Potential Energy) and CIN (Convective INhibition) via integration from the Level of Free Convection  $z_{LFC}$  and the Level of Zero Buoyancy  $z_{LZB}$ .

$$\begin{cases} \text{CAPE} = g \int_{z_{LFC}}^{z_{LZB}} \frac{T_c - T_{env}}{T_{env}} dz \\ \text{CIN} = -g \int_{z_0}^{z_{LFC}} \frac{T_c - T_{env}}{T_{env}} dz \end{cases} \quad (4.6)$$

CAPE is used to measure the atmospheric instability due to buoyancy forces, and by consequence the updraft formation capacity. CIN on the other hand, gives a measure on atmospheric capping, which inhibits updrafts.

Strong storms are usually formed when high levels of CAPE ( $\geq 1000 \text{ J/kg}$ ) are measured, but also a high value of CIN can contribute to storm formation, as the presence of a cap can favor deep convection in case of atmospheric cooling and the “dissolution” of the aforementioned cap. Both values can be measured easily via atmospheric soundings with radiosondes, as in figure A.2

Both parameters can be evaluated using virtual temperature, accounting for water-vapor mixing, and are known in literature as CAPV and CINV. Other parameters that can be used to determine and forecast storm strength can be determined from storm modeling, such as the Bulk Richardson number  $R_B$  and the non dimensional storm strength  $S$ .

The first of the two is defined as for [8]

$$R_B = \frac{\text{CAPE}}{(\Delta V)^2 / 2} \quad (4.7)$$

Where  $\Delta V$  is defined as the difference of the mid level ( $p \approx 500 \text{ hPa}$ ) density-weighted average wind speed and the average near-surface layer wind speed ( $p \approx 1000 \text{ hPa}$ ). This accounts for shear and it's therefore possible to estimate the storm type that might form. From observations, values of  $10 < R_B < 50$  support supercell formation

and  $R_B > 50$  support multicellular storm formation. In the sounding in figure A.2 it's indicated as BRCH (BRCV uses CAPV) and supports multicellular storm formation.

The non dimensional storm strength  $S$  is strictly dependent on numerical models, and is defined as for [8]

$$S = \frac{w_{max}}{\sqrt{2\text{CAPE}}} \quad (4.8)$$

Where  $w_{max}$  is the simulated maximum vertical velocity, and CAPE is the theoretical maximum vertical velocity for a certain CAPE value as  $w_{max,i} = \sqrt{2\text{CAPE}_i}$ .

### §§ 4.2.2 Storm Splitting

The formation and development of supercell storms can be explained directly using (4.2). Considering a purely rotational horizontal flow for which  $\partial_x v = -\partial_y u$ , we have [8, 14]

$$\frac{\partial v}{\partial x} \frac{\partial u}{\partial y} = -\frac{1}{4} \zeta^2$$

And thus, in a strong vortex

$$\nabla^2 p'_d \propto -p'_d \propto \zeta^2 \quad (4.9)$$

Indicating the presence of a dynamic pressure perturbation minimum associated with the vortex, thus indicating that midlevel rotation acts to lower pressure at midlevels on the storm flanks.

Considering that supercell storms form in strong environmental shear conditions, taken a constant average wind  $\mathbf{v}_{env} = (u_{env}, v_{env}, 0)$ , and defining the vertical shear vector as [14]

$$\mathbf{S} = \frac{\partial \mathbf{v}_{env}}{\partial z} \quad (4.10)$$

We can then modify the dynamical pressure perturbation equation as

$$\nabla^2 p'_d = -2\rho_s \mathbf{S} \cdot \nabla_H w \quad (4.11)$$

Indicating that there will be a maximum of pressure gradient divergence in the zone of strong horizontal gradient of vertical velocity on the downshear side of the updraft.

This effect favors the reproduction of supercell storms via splitting of the updraft into two (usually unequal in strength) updrafts. From observations in the continental United States, in supercell storm events the windshear stretches and rotates with height, in a clockwise fashion, favoring the cyclonic “right mover” supercell that forms from the split.

### §§ 4.2.3 Updraft Rotation and Supercell Tornadogenesis

The rotating nature of the updraft can be quickly explained by the evaluation of a supercell storm in an unidirectional shear environment. Said  $\mathbf{c} = (u_c, v_c)$  the storm propagation velocity vector and considered  $u_c = U$  at the level of no divergence,

from the vorticity equation on the  $yz$  plane in a steady state condition,  $\partial_t \zeta' = 0$ ,  $\partial_y \zeta' = \zeta'$ ,  $\partial_y w = w$  [8]

$$\zeta' = -\frac{w}{v_c} \frac{\partial U}{\partial z} \quad (4.12)$$

Indicating that the southward moving storm will have positive vorticity whenever  $\partial_z U > 0$ , and its maximum will coincide with the maximum of  $w$ , thus explaining the strong rotation of the updraft of a supercell.

The strong rotation of the updraft in a storm, if some conditions are met, can generate a rotating mesovortex, which itself might form a tornado. A mesovortex is formed usually when the following conditions are met:

- Rapid increase of low level rotation
- Decrease in updraft intensity
- Formation of a rear flank downdraft (RFD) behind the rotating updraft
- Low level inflow of air towards higher levels in a high windshear environment

The subsequent formation of the mesovortex can then generate a tornado when there is a high buoyancy at the surface (measurable via CAPE measurements), high conditional instability towards the RFD and a CIN decrease at the RFD. If then the tornado is formed at the mesovortex location, visually described by meteorological RADARs as a hook echo in the WER (or BWER, if strong) region, it's sometimes possible to observe a strong increase of windshear at midlevels, known as a Tornadic Vortex Signature or TVS.

The dynamics of the tornadic vortex can then be explained using the vertical component of the Navier-Stokes equations for an inviscid, homogeneous and adiabatic flow together with the cyclostrophic relations [8]

$$\begin{cases} \frac{\partial w}{\partial t} + \mathbf{v} \cdot \nabla w = -\frac{1}{\rho_s} \frac{\partial p}{\partial z} \\ \frac{v^2}{r} = \frac{1}{\rho_s} \frac{\partial p}{\partial r} \end{cases} \quad (4.13)$$

Considering cylindrical coordinates and taking the radial derivative of the first equation, one obtains the equations of motion for tornadic flow

$$\frac{\partial^2 w}{\partial r \partial t} + \frac{\partial}{\partial r} (\mathbf{v} \cdot \nabla w) = -\frac{\partial}{\partial z} \left( \frac{v^2}{r} \right) \quad (4.14)$$

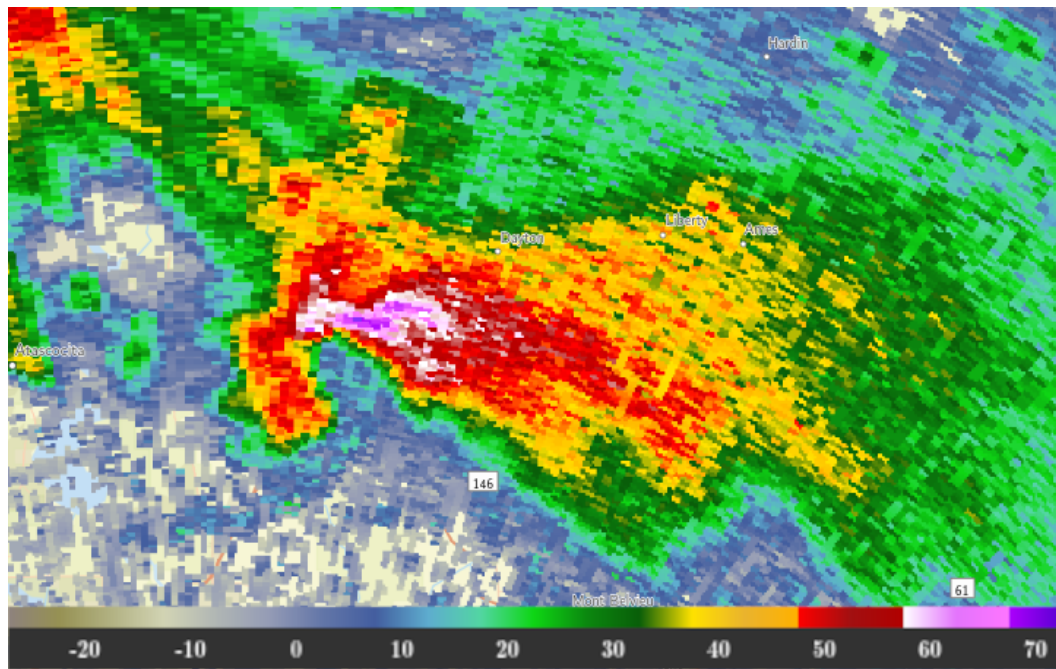


**Figure 4.3.** KHGX WSR-88D RADAR reflectivity imagery of a supercell storm exhibiting a strong mesovortex and a BWER region in Houston, Texas, which prompted a tornado warning from the National Weather Service for Stilson, TX, 2 May 2025. Scale in dBZ [18]

# 5. Front and Jet Dynamics

---

## § 5.1 Frontogenesis

---

### §§ 5.1.1 Thermodynamics and Kinematics of Frontogenesis

A meteorological front is defined as the boundary of two airmasses with different densities. A front can be modeled using a basic wedge model via the evaluation of the slope of its slope. Noting the density of the warmer airmass as  $\rho_w$  and the density of the colder airmass as  $\rho_c$ , we have [8]

$$\frac{dz}{dy} = \frac{1}{g(\rho_c - \rho_w)} \left[ \left( \frac{\partial p}{\partial y} \right)_c - \left( \frac{\partial p}{\partial y} \right)_w \right] \quad (5.1)$$

Since fronts tend to be in the meso- $\alpha$  scale in length and on meso- $\beta$  in width [7], we can assume that the lengthwise winds are in geostrophic balance. Using the geostrophic wind equations and Mergules formula [8], we have

$$\frac{dz}{dy} = \frac{f \langle T \rangle}{g(T_w - T_c)} (u_{gw} - u_{gc}) \quad (5.2)$$

Where  $\langle T \rangle$  is average temperature across the front

From this equations it's possible to then determine the average shear and vorticity across the front.

A more generic function to determine frontogenesis or frontolysis, considering thermodynamic variables, was found by Miller in 1948 [3] as

$$F_M = \left( \frac{\partial}{\partial t} + \mathbf{v} \cdot \nabla \right) \|\nabla \theta\| = \frac{\nabla \theta}{\|\nabla \theta\|} (\nabla \dot{Q} - \nabla \mathbf{v} \cdot \nabla \theta) \quad (5.3)$$

Where the thermodynamic equation  $\dot{\theta} = \dot{Q}$  was used in order to rewrite the function. This function indicates whether the thermodynamic conditions are met for frontogenesis depending on the sign of  $F_M$ , with  $F_M > 0$  indicating favorable conditions. Note that  $\nabla \dot{Q}$  are the differential heating terms and  $\nabla \mathbf{v} \cdot \nabla \theta$  are the shearing and stretching deformations of the airmasses.

### §§ 5.1.2 Cross-frontal Circulations and the Sawyer-Eliassen Equation

As we have indicated in the previous section, the typical scales of fronts permit us to consider winds across the front as perturbations to the geostrophic wind balance.

Considered a simplified front which runs along the x-axis, given the geopotential function  $\Phi$ , across the  $y$  axis we have, if we consider  $\hat{\mathbf{v}} = \mathbf{v}_g + \mathbf{v}_a$  with  $\mathbf{v}_g = (u_g, v_g)$  being the geostrophic wind and  $\mathbf{v}_a = (u_a, v_a)$  being the ageostrophic correction [8]

$$\frac{\partial v_g}{\partial t} + \mathbf{v} \cdot \nabla v_g = -fu - \frac{\partial \phi}{\partial y} = -fu_a = 0 \quad (5.4)$$

Thus leading to  $\hat{\mathbf{v}} = (u_g, v_g + v_a)$ , and redefining the velocity field of the fluid in three dimensions in the quasi-geostrophic approximation as  $\tilde{\mathbf{v}} = (u_g, v_g + v_a, w)$ . Considering the geostrophic momentum equations found by [5],

$$\begin{cases} \nabla_H \Phi = -f\hat{\mathbf{k}} \times \mathbf{v}_g \\ \frac{\partial \Phi}{\partial z} = g \frac{\theta}{\theta_0} = b \end{cases} \quad (5.5)$$

We reach the thermal wind balance equations

$$f \frac{\partial \mathbf{v}_g}{\partial z} = -\hat{\mathbf{k}} \times \nabla_H b \quad (5.6)$$

Imposing the conservation of the thermal wind balance in the quasi-geostrophic approximation on equation (5.4) and on the thermodynamic equation, we obtain [8]

$$\begin{cases} \left( \frac{\partial}{\partial t} + \tilde{\mathbf{v}} \cdot \nabla \right) \left( f \frac{\partial u_g}{\partial z} \right) = Q_2 + f \left( f - \frac{\partial u_g}{\partial y} \right) \frac{\partial v_a}{\partial z} - \frac{\partial v_a}{\partial y} \frac{\partial b}{\partial y} \\ \left( \frac{\partial}{\partial t} + \tilde{\mathbf{v}} \cdot \nabla \right) \left( -\frac{\partial b}{\partial y} \right) = -Q_2 + \frac{\partial w}{\partial y} \frac{\partial b}{\partial z} + \frac{\partial v_a}{\partial y} \frac{\partial b}{\partial y} - \frac{g}{\theta_0} \frac{\partial \dot{Q}}{\partial y} \\ Q_2 = -\frac{\partial u_g}{\partial y} \frac{\partial b}{\partial x} - \frac{\partial v_g}{\partial y} \frac{\partial b}{\partial y} \end{cases} \quad (5.7)$$

It's of particular interest that if  $v_a = 0$ , and thus the wind is considered in geostrophic balance on the x and y directions,  $Q_2 > 0$  would indicate an increase of vertical shear on  $u_g$  and a decrease of  $\partial_y b$  for the first equation, creating a frontolytic situation, while indicating a frontogenetic situation on the second, thus imposing the need of the ageostrophic corrections for maintaining thermal wind balance.

Equating (5.7), imposing thermal wind balance and noting that the ageostrophic circulation lies only on the  $yz$  plane, it's possible to define a streamfunction  $\psi$  as

$$\begin{cases} v_a = -\frac{\partial \psi}{\partial z} \\ w = \frac{\partial \psi}{\partial y} \end{cases} \quad (5.8)$$

Which, if substituted inside with what was obtained, yields the Sawyer-Eliassen equation [4, 5]

$$N^2 \frac{\partial^2 \psi}{\partial y^2} + 2S^2 \frac{\partial^2 \psi}{\partial y \partial z} + F^2 \frac{\partial^2 \psi}{\partial z^2} = 2Q_2 + \frac{g}{\theta_0} \frac{\partial \dot{Q}}{\partial y} \quad (5.9)$$

Where

$$N^2 = \frac{\partial b}{\partial z}, \quad S^2 = -\frac{\partial b}{\partial y} = f \frac{\partial u_g}{\partial z}, \quad F^2 = f \left( f - \frac{\partial u_g}{\partial y} \right) \quad (5.10)$$

If these coefficients are known, it's possible to find an unique solution for  $\psi$  provided that the elliptic condition for the potential vorticity  $PV = N^2 F^2 - S^4 > 0$  is satisfied. This quantity is conserved along the fluid motion

## § 5.2 Jet Streaks

---

### §§ 5.2.1 Jetogenesis and Lateral Secondary Circulations

A jet streak, also known as an upper-level front, is a narrow and long zone often associated with the polar-front jet streak, a long and narrow high level mesoscale boundary in which wind speeds of up to 220 KTS have been measured. [8].

The knowledge of jet streak generation and decay is fundamental in weather forecasting and aviation, where intercontinental high-level routes are chosen following jet streak forecasts. The generating function of jet streaks can be evaluated similarly to fronts, where the potential temperature is substituted by the wind field strength in the jet core  $\nabla^2 u$  [7]

$$F_j = - \left( \frac{\partial}{\partial t} + \mathbf{v} \cdot \nabla \right) \nabla^2 u = -\nabla^2 \left[ \frac{\partial u}{\partial t} + \mathbf{v} \cdot \nabla u + \nabla^2 (\mathbf{v} \cdot \nabla u) - (\mathbf{v} \cdot \nabla) \nabla^2 u \right] \quad (5.11)$$

Imposing the quasi-geostrophic approximation and considered  $\nabla u = 0$  in the center of the jet and uniform near the air parcel we have

$$F_j = -f \nabla^2 v_a - 2 \frac{\partial f}{\partial y} \frac{\partial v_a}{\partial y} \quad (5.12)$$

In midlatitudes the second term is negligible, noting that  $\partial_y f \approx 0$ .

Defined the kinetic energy of the air parcel as  $K = \frac{1}{2} (u^2 + v^2)$ , we have in frictionless conditions [7]

$$\frac{\partial K}{\partial t} + \mathbf{v} \cdot \nabla K = -\mathbf{v} \cdot \nabla \Phi \quad (5.13)$$

The positivity of the right hand side indicates a wind velocity deflection towards lower pressures, i.e. the ageostrophic component of the wind is directed towards the lower pressure.

Considered a westerly jet streak together with the kinetic energy equation (5.13), it's possible to find that the largest increment of kinetic energy happens inside the jet, while on the southern and northern side we have respectively convergence and divergence on the  $yz$  plane, due to the presence of the minima and maxima of the ageostrophic  $v_a$  component thanks to the acceleration of the air parcels along the streamlines, causing a secondary vertical circulation.

Considering a westerly jet streak on the northern hemisphere, we will colder air on the northern side of the jet and warmer air on the southern side of the jet, thus indicating that the secondary circulation is a lateral thermal circulation which converts AAPE (Available Atmospheric Potential Energy) into kinetic energy in the southern side and vice versa on the northern side. This secondary circulation can also be explained via frontogenesis, as in the entrance region of the jet we must have  $\partial_x u_g > 0$  and  $\partial_y \theta < 0$ , and the inverse on the exit region, indicating the presence of a frontal region.

### §§ 5.2.2 Upper-Lower Level Jet Streak Coupling and Severe Storms

Jet streams in midlatitudes are usually confined to higher levels ( $p \approx 300$  mbar [8]), but the formation of lower level intra-boundary layer jet streaks is possible. These low level jets are fundamental for explaining severe convective storms and mesoscale convective complexes that commonly form in the warm seasons in the central plains of the USA, Argentina and South East Asia.

Uccellini and Johnson (1979) [6] indicated that the formation of these deep convective complexes can be explained via the coupling of the secondary lateral circulations of upper level and lower level jet streaks.

Considered the quasi-geostrophic approximation equation, the ageostrophic component of the wind velocity is found to be equal to the geostrophic material derivative of the geostrophic wind.

$$f\mathbf{v}_a = \hat{\mathbf{k}} \times \left( \frac{\partial \mathbf{v}_g}{\partial t} + \mathbf{v}_g \cdot \nabla \mathbf{v}_g \right) \quad (5.14)$$

At low levels, in the entrance of the upper level jet, the ageostrophic wind will point towards the higher pressure side and vice-versa in the exit region. This corresponds to the condition  $-\mathbf{v} \cdot \nabla \Phi > 0$ , thus indicating an increase of low level kinetic energy and the formation of a low level jet, which can couple with the upper jet in both the entrance and exit regions of the former.

Considering an entrance region coupling, where the jets are parallel, the result will be two dependent secondary circulations, while on the exit side, where the jets are perpendicular, the formation of an indirect secondary lateral thermal circulation. For a westerly jet streak on the northern hemisphere thus, at the left side of the low level jet deep convection will be favored due to the conversion of AAPE into kinetic energy.

A major example of this phenomenon happens in the plains of the southern United States, where a seasonal low level jet transports warm humid air northwards from the Gulf of Mexico couples with the easterly upper jet streak causing deep convection, and in the worst situations, squall lines of tornado-capable supercells, permitting an event commonly known as tornado outbreaks.

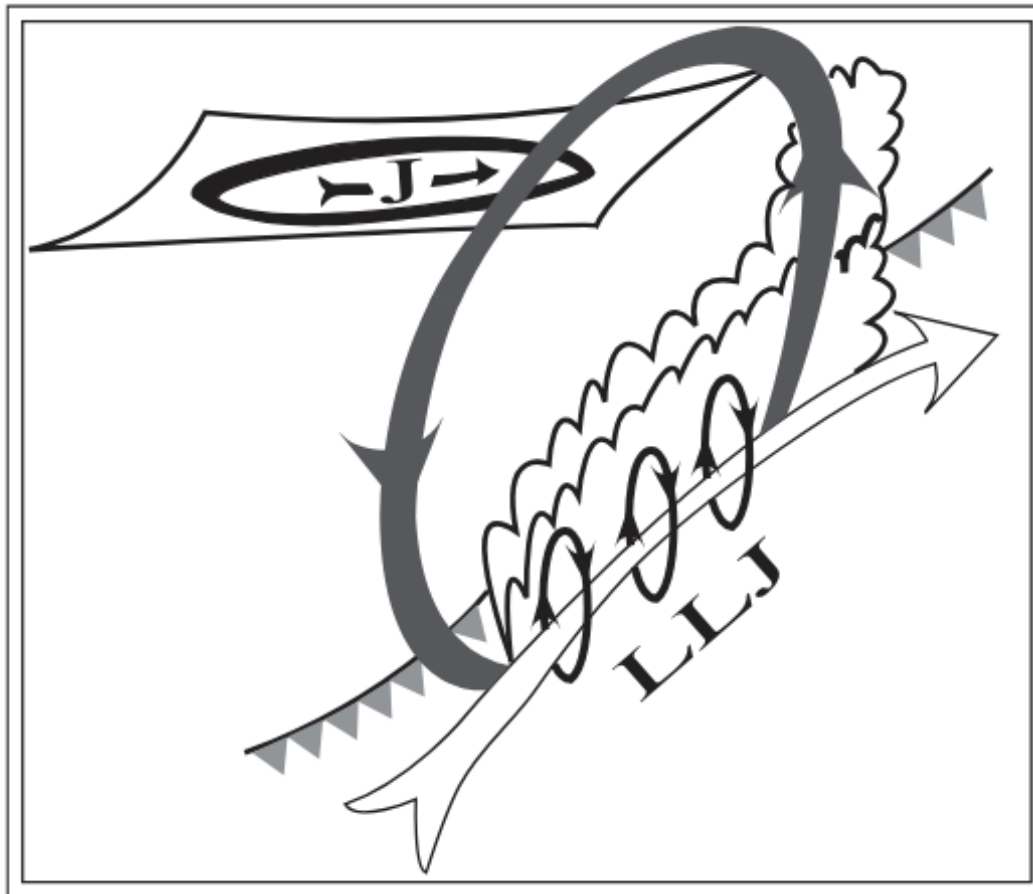


**Figure 5.1.** Schematics of upper level-low level jet streak lateral secondary circulation coupling and its contribution to deep convection.  $J$  indicates the upper level jet and  $LLJ$  indicates the lower level jet. Taken from [8]

## 6. Conclusions

---

In this thesis, a theoretical framework of mesoscale phenomena has been developed starting from the fundamental equations of atmospheric dynamics and applying appropriate, scale-dependent, approximations, with which a set of perturbative mesoscale equations has been derived.

In treating forced orographic flows, the perturbative equations have been reduced into the Scorer equation (3.2) and coupled with appropriate boundary conditions that describe mathematically the ground elevation, a full description of the linear theory of mountain waves has been described, including the relationship between the Scorer parameter  $l(z)$  (3.3) and the possible regimes of mountain waves. This evaluation permitted the generalization of the phenomenon to mountain ranges with mesoscale dimensions, where a quasi-geostrophic treatment permitted to describe the particular phenomenon of Alpine cyclogenesis.

The subsequent chapter described cumulus convection and storm formation in terms of pressure and vorticity perturbations, converging towards a description of the dynamics of supercell storms and giving an introduction to supercell tornadogenesis, indicating how the mesoscale perturbations on pressure can describe storm splitting in high shear environment and the eventual formation of tornadoes.

The last chapter describes front formations, first modeling fronts using a wedge model and then deriving the Sawyer-Eliassen equation (5.9) in the quasi-geostrophic framework, indicating then the necessity of a positive potential vorticity for frontogenesis and the existence of secondary lateral circulations in fronts. Successively, jet streaks have been modeled as high-level fronts, deriving an analogue to the Miller frontogenesis function (5.3) for jetogenesis (5.12).

Including energetic considerations, lateral secondary circulations for jet streaks and interactions with low level jets, a framework for explaining deep convective storm outbreaks in the American plains has been described.

This description, even if useful in the description of severe weather events and forced orographic circulations, remains incomplete without the inclusion of interactions with the atmospheric boundary layer and with oceans. The complexity of equations and the need of including detailed elevation models makes forecasting in the mesoscale a complex and computationally expensive task, but still fundamental

in disaster preparedness and global aviation.

Specifically in the case of mountain waves and jet streaks, their forecasting is fundamental in reducing turbulence related injuries. As per the 2021 National Transportation Safety Board (NTSB) Safety Research Report [19], both phenomena have caused such incidents (via clear air turbulence or directly for mountain waves). Excluding aviation, the forecasting of severe convective storms is paramount to the safety of everyone, where advanced alerts of strong storms help with reducing fatalities and severe injuries due to flash flooding, strong hailstorms and tornadoes.

# A. Additional Figures

## § A.1 Orographic Flows

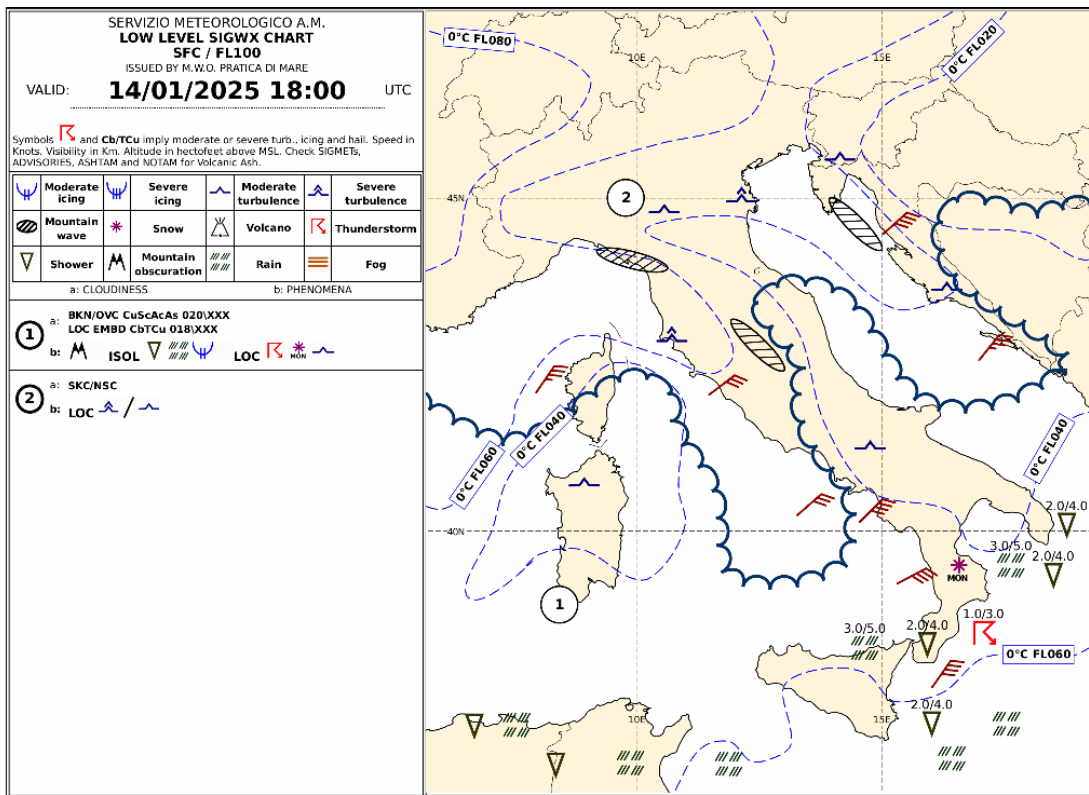


**Figure A.1.** SWLL Chart from the meteorological service of the Italian Air Force, valid 14 January 2025, 18:00±3:00 UTC (Universal Coordinated Time)

This chart describes the SWLL (Low Level Severe Weather) forecast for the Italian peninsula, valid January 14 2025 at 18:00±3:00, Unified Coordinated Time, forecasting mountain waves where rotor clouds were observed via Copernicus imagery the same day, as in figure

3.1. The forecast on the left describes using international cloud codes and international coding for phenomena, two zones. The second zone, which is the one in study, gives a SKC/NSC (clear sky/no significative clouds) and local moderate to severe turbulence. In the chart, three zones of mountain waves are indicated over the area, specifically over the gulf of Genoa, over the Dalmatian coast of Croatia and over the imaged Umbria region. Note that the forecast is valid from SFC (surface) till FL100 (10000 ft of altitude from the standard pressure of 1013.25 hPa)

## § A.2 Severe Storms

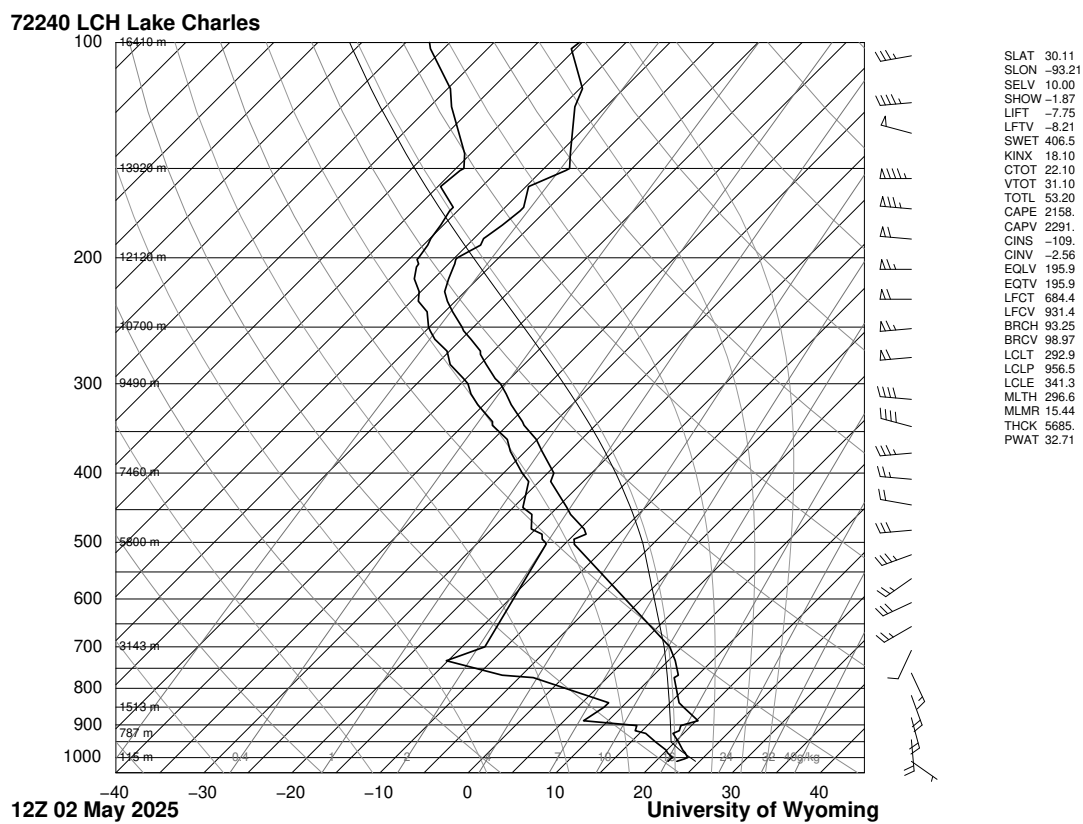


**Figure A.2.** Skew-T diagram of an atmospheric sounding before a severe thunderstorm outbreak in Louisiana, Texas and Mississippi, May 2 2025. The station is located in Lake Charles Regional Airport, Louisiana (ICAO code KLCH) [20]

This diagram shows the vertical temperature and wind profile in the area of KLCH at 12:00 UTC from which various indexes have been evaluated, such as CAPE (2158 J/kg), CAPV (2291 J/kg), CIN (-109 J/kg), CINV (-2.56 J/kg) and  $R_B$  (93.25), which have been

defined in section 4.2.1. Other parameters are also evaluated from the profile and indicated in the right, giving a comprehensive evaluation, such as the K-index (KINX), the Total totals index (TOTL), the Showalter index (SHOW), the Lifted index (LIFT, LFTV) and the Severe Weather Threat index (SWET).

# Bibliography

---

- <sup>1</sup>R. S. Scorer, “Theory of airflow over mountains: iii - airstream characteristics”, Quarterly Journal of the Royal Meteorological Society **80**, 417–428 (1954).
- <sup>2</sup>S. Tibaldi, A. Buzzi, and A. Speranza, “Orographic cyclogenesis”, in «*Extratropical cyclones: the erik palmén memorial volume*», edited by C. W. Newton and E. O. Holopainen (American Meteorological Society, Boston, MA, 1990), pp. 107–127.
- <sup>3</sup>J. E. Miller, “On the concept of frontogenesis”, Journal of the Atmospheric Sciences, 169–171 (1948).
- <sup>4</sup>J. S. Sawyer, “The vertical circulation at metereological fronts and its relation to frontogenesis”, Proceedings of the Royal Society A, Mathematical, Physical and Engineering Sciences, 10.1098/rspa.1956.0039 (1956).
- <sup>5</sup>A. Eliassen, “On the vertical circulation in frontal zones”, Geofysiske Publikasjoner (1962).
- <sup>6</sup>L. W. Uccellini and D. R. Johnson, “The coupling of upper and lower tropospheric jet streaks and implications for the development of severe convective storms”, Monthly Weather Review, 10.1175/1520-0493(1979)107<0682:TCOUAL>2.0.CO:2 (1979).
- <sup>7</sup>S. Shou, S. Li, Y. Shou, and X. Yao, «*An introduction to mesoscale meteorology*» (Springer Nature and China Meteorological Press, 2023).
- <sup>8</sup>Y. L. Lin, «*Mesoscale dynamics*» (Cambridge University Press, 2007).
- <sup>9</sup>K. A. Emanuel, «*Overview and definition of mesoscale meteorology*», edited by P. S. Ray (American Meteorological Society, Boston, MA, 1986).
- <sup>10</sup>J. R. Holton and G. J. Hakim, «*An introduction to dynamic meteorology*», 5th ed. (Academic Press, 2012).
- <sup>11</sup>R. S. Scorer, “Theory of waves in the lee of mountains”, Quarterly Journal of the Royal Meteorological Society **75**, 41–56 (1949).
- <sup>12</sup>R. S. Scorer, “Theory of airflow over mountains: ii - the flow over a ridge”, Quarterly Journal of the Royal Meteorological Society **79**, 70–83 (1953).
- <sup>13</sup>“Sentinel 2 l2a imagery”, Copernicus Project (2025).

- <sup>14</sup>jr. Robert A. Houze, «*Cloud dynamics*», 2nd ed., International Geophysics (Academic Press, 2014).
- <sup>15</sup>“Thunderstorm formation”, NOAA (2010).
- <sup>16</sup>M. Janoušek, “Večerní kupy 15. 6. 2016”, Amatérská Meteorologická Společnost (2016).
- <sup>17</sup>M. Janoušek, “Večerní kupy 15. 6. 2016”, Amatérská Meteorologická Společnost (2016).
- <sup>18</sup>“Local radar for super resolution for base reflectivity”, NOAA National Weather Service (2025).
- <sup>19</sup>“Safety research report: preventing turbulence-related injuries in air carrier operations conducted under title 14 cfr part 121”, National Transportation Safety Board (2021).
- <sup>20</sup>“Atmospheric soundings”, Department of Atmospheric Sciences, University of Wyoming (2025).
- <sup>21</sup>L. D. Landau and E. M. Lifshits, «*Volume 6, fluid mechanics*», 2nd ed., Course of Theoretical Physics (Pergamon Press, 1987).
- <sup>22</sup>S. Pettersen, «*Volume 1, motion and motion systems*», 1st ed., Weather Analysis and Forecasting (McGraw-Hill Book Co., 1956).
- <sup>23</sup>“Low level significant weather chart”, Servizio Meteorologico Aeronautica Militare, MWO Pratica di Mare (2025).